JACS
JOURNAL OF THE AMERICAN CHEMICAL SOCIETY

Communication

pubs.acs.org/JACS

Deposition, Characterization, and Thin-Film-Based Chemical Sensing of Ultra-long Chemically Synthesized Graphene Nanoribbons

Ahmad N. Abbas,[‡,⊥,§] Gang Liu,[‡,§] Akimitsu Narita,[†] Manuel Orosco,[¶] Xinliang Feng,[†] Klaus Müllen,[†] and Chongwu Zhou*[,‡]

[‡]Department of Electrical Engineering, University of Southern California, Los Angeles, California 90089, United States

[†]Max Planck Institute of Polymer Research, Ackermannweg 10, 55128 Mainz, Germany

[¶]Alfred E. Mann Institute for Biomedical Engineering, University of Southern California, Los Angeles, California 90089, United States

[⊥]Department of Electrical Engineering, King Abdulaziz University, Abdullah Sulayman Street, Jeddah 22254, Saudi Arabia

Supporting Information

ABSTRACT: Bottom-up synthesis of graphene nanoribbons (GNRs) is an essential step toward utilizing them in electronic and sensing applications due to their defined edge structure and high uniformity. Recently, structurally perfect GNRs with variable lengths and edge structures were created using various chemical synthesis techniques. Nonetheless, issues like GNR deposition, characterization, electronic properties, and applications are not fully explored. Here we report optimized conditions for deposition, characterization, and device fabrication of individual and thin films of ultra-long chemically synthesized GNRs. Moreover, we have demonstrated exceptional NO_2 gas sensitivity of the GNR film devices down to parts per billion (ppb) levels. The results lay the foundation for using chemically synthesized GNRs for future electronic and sensing applications.

Theoretical predictions of quantum confinement in a graphene lattice have driven extensive research to verify that such confinement can be experimentally realized to create an energy bandgap in graphene.[1,2] The creation of a bandgap in graphene is essential for the utilization of graphene in digital integrated circuits so that switching off the channel can be realized. Recently, much effort was put into generating GNRs with various widths and lengths using lithographic,[3−5] chemical,[6−8] and various other techniques.[9−17] However, patterning graphene using top-down approaches creates GNRs with rough edges, which can degrade the carrier transport.[18] Accordingly, the inability to create GNRs with specific edge structures results in significant sample-to-sample variations and disagreement with theoretical predictions on electronic properties.[1]

To overcome such problems, various bottom-up chemical methods were developed to control the width and edge structure of such GNRs with high uniformity.[19−27] These methods allow very controllable tuning of the electronic edge structure of GNRs with the possibility of large-scale synthesis, which is desirable for future electronic and sensing applications of GNRs. Moreover, the latest advancement in chemical synthesis allowed the creation of ultra-long (>200 nm) GNRs that are even processable in the liquid phase, thus facilitating the utilization of such GNRs in various applications.[28] Nevertheless, some challenges such as GNR deposition (i.e., both isolated individual GNRs and thin films), characterization, and electronic device measurements are not fully explored.

Here we report optimized conditions for deposition and visualization of individual bottom-up chemically synthesized GNRs and films on Si/SiO_2 substrates and their applications as devices and chemical sensors. This is in contrast to a previous report,[28] where deposition of GNRs was performed only on conductive substrates and could not be directly applied for device studies. Other works, reporting electronic investigation of individual GNRs, employed top-down fabricated GNRs,[6−8] which might have been significantly affected by non-uniform width and undefined edge structures. We have studied different annealing conditions and their effect on GNR thin-film devices using attenuated total reflectance Fourier transform infrared (ATR-FTIR) spectroscopy, electrical measurements, and Raman spectroscopy. Additionally, we have demonstrated an application of the GNR thin-film devices by measuring the sensitivity of such GNRs to NO_2 gas and observed ppb-level sensitivity, highlighting the potential for using chemically synthesized GNRs for cost-conscious and scalable sensing applications.

Figure 1a shows the structure of the GNRs used in this study, which were synthesized using recently reported methods.[23,28] These GNRs have cove-type edge structures with width dimensions of 1.1 and 0.7 nm (Figure 1a). GNRs **1a** and **1b** bear dodecyl and *tert*-butyl groups, respectively, at the edges, which contribute to their enhanced processability. Additionally, based on the weight-average molecular weight of corresponding polyphenylene precursors, the average length of such GNRs can be estimated to be ∼500 and ∼390 nm for GNRs **1a** and **1b**, respectively.[23,28] Dispersions of GNRs in solvents are usually prepared by sonicating GNR powder in the solvent, followed by centrifugation (Note s1). Figure s1 shows the ultraviolet−visible absorption spectra of GNRs **1a** and **1b** dissolved in various solvents. Moreover, the optical bandgap of the GNRs can be extrapolated from Figure s1, which yields a value of ∼1.84 eV, comparable to theoretical predictions and other reports.[28,29]

Received: March 18, 2014
Published: May 15, 2014

   dx.doi.org/10.1021/ja502764d | J. Am. Chem. Soc. 2014, 136, 7555−7558

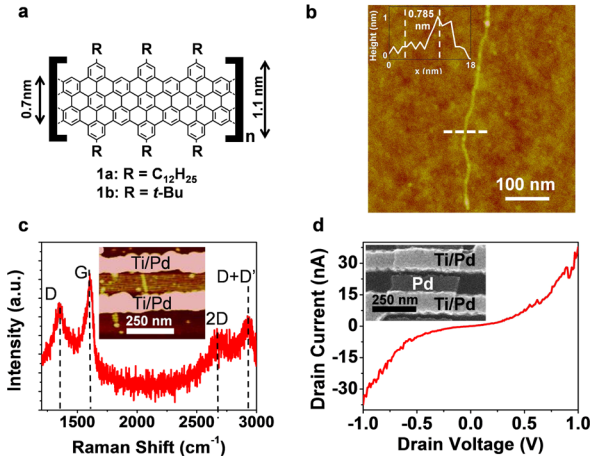

Figure 1. (a) Chemical structure of GNRs **1a** and **1b**. (b) AFM tapping-mode height image revealing synthesized GNR length >500 nm. Inset shows a height profile of the GNR (at the dashed line) revealing a height of 0.785 nm. (c) Raman spectrum of an individual GNR revealing D, G, 2D, and D+D′ bands. Inset shows an individual GNR between two Ti/Pd electrodes. (d) Current vs drain voltage (I–V_d) characteristic of an individual GNR device after metal angle deposition with a channel length of ∼20 nm. Inset shows an SEM image of a 20 nm gap between Ti/Pd and angle-deposited Pd.

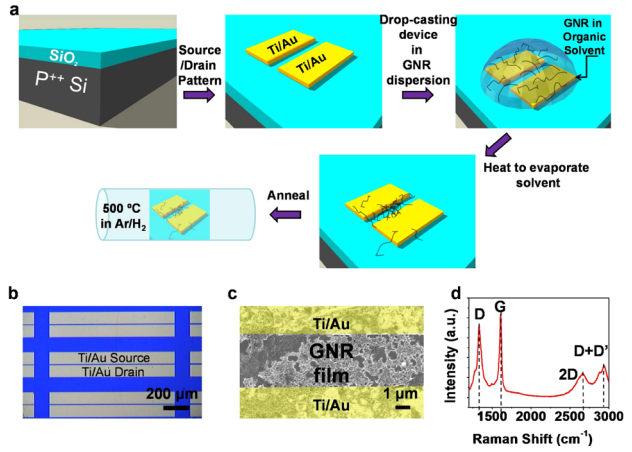

Figure 2. (a) Scheme of GNR film device fabrication. (b) Optical image of the fabricated devices. (c) SEM image of a typical GNR film device with GNR films between two (falsely colored) Ti/Au electrodes. (d) Raman spectrum of GNR films showing D, G, 2D, and D+D′ bands, in agreement with a single GNR Raman spectrum.

Because the GNRs are long and have extended aromatic structures, strong interactions between GNRs cause their aggregation in the solvent, which can be visually observed as partial precipitation in the dispersions in solvents such as chlorobenzene (CB) and tetrahydrofuran (THF), depending on the concentration and duration after preparation. Despite the successful synthesis of GNRs **1a** and **1b**, deposition and visualization of such individual GNRs on various substrates has not been previously achieved. To image and characterize individual GNRs on a substrate of choice, aggregation of GNRs in the dispersion should be minimized while adhesion to the substrate must be promoted by proper surface functionalization. Additionally, it is preferable to have a solvent with a high boiling point so that long incubation times are possible. Based on those requirements, we functionalize the surface of a Si/SiO_2 wafer with dodecyltriethoxysilane while using 1-cyclohexyl-2-pyrrolidone (CHP) as a solvent for GNR incubation on the functionalized wafer for 24 h (Note s1). CHP has a boiling point of ∼290 °C at atmospheric pressure, and we have observed that GNR dispersions in CHP are very stable, with little visible precipitation for the time frame of 10 days, in sharp contrast to those in CB and THF. Figure 1b shows a typical atomic force microscope (AFM) image of a GNR with length >500 nm and height ∼0.78 nm on the functionalized SiO_2 surface. Considering the error corresponding to AFM tip radius (i.e., ∼2 nm, see Note s1), the observed width of ∼5.0–6.9 nm is consistent with the expected value for a single GNR **1a** including the alkyl chains (∼3.8 nm). Additionally, most GNRs observed by AFM were 300–500 nm long (Figure s2). To locate individual GNRs for recording a Raman spectrum, the measurement was done by patterning two Ti/Pd electrodes on an individual GNR (deposited using CHP as a solvent) using electron beam lithography and subsequently focusing the laser on the located GNR (Figure 1c). The spectrum shows clear D, G, 2D, and D+D′ peaks, which is consistent with GNR thin films (Figure 2d) and a previously reported spectrum measured on a powder sample of GNR **1a**.[21,28] Electrical measurements on an individual GNR with a channel length of ∼100 nm (Figure 1c inset) revealed little current conduction in the GNR. Subsequently, we performed metal angle deposition to shorten the channel length to ∼20 nm (Figure 1d inset) and observed current conduction in the GNR (Figure 1d), which confirms the conductivity of GNR **1a** (Note s2).

We have fabricated GNR thin-film devices by drop-casting the dispersion of GNR **1a** in THF or CB, as demonstrated in Figure 2a. First, 1 nm Ti/50 nm Au electrodes are patterned on top of P^{++} Si/300 nm SiO_2 substrate (Figure 2 a,b). The GNR dispersion (Note s1) is then dropped on top of the substrate while the substrate is heated to 120 °C to evaporate the solvent. Here, we used THF or CB as the solvent because they can vaporize rapidly and leave a GNR film behind, while CHP has a high boiling point and is suitable for incubation to get individual GNRs. Afterward, the substrate is annealed in H_2/Ar gases (Note s1). Figure 2c shows a scanning electron microscope (SEM) image of a GNR film between two Ti/Au electrodes for device study. Moreover, deposition of the GNRs was confirmed by Raman analysis (Figure 2d).[19,21,28]

The annealing step after drop-casting the GNR is crucial to enhance the conductivity of GNR film devices. The motivation behind annealing the GNR films was to cut off the insulating alkyl chains from the GNR edges to reduce ribbon-to-ribbon junction resistance without affecting the basal plane.[30] To characterize the annealing effect on the GNR film, ATR-FTIR measurements were carried out on GNR films at different annealing temperatures (Figure 3a,b and Figure s4). The spectra were normalized to the peak from conjugated C–C at ∼1600 cm^{-1}. The clear decrease of the alkyl C–H peaks (i.e., ∼1380, 1470, and 2850–2925 cm^{-1}) relative to the conjugated C–C peak after annealing at 400 and 500 °C (Figure 3a,b) suggests the partial removal of alkyl chains from the GNR edges at such conditions. Additionally, the disappearance of the peak at ∼720 cm^{-1}, which is also a characteristic peak for alkyl chains, further confirms the removal of alkyl chains from GNR edges (Figure s4).[28] On the other hand, the peak at ∼863 cm^{-1}, which corresponds to C–H bonds at the cove position of GNR,[28] is maintained, which suggests minimal damage to the GNR basal plane after thermal treatment. Moreover, Raman spectroscopy of GNR films after different annealing conditions

dx.doi.org/10.1021/ja502764d | J. Am. Chem. Soc. 2014, 136, 7555–7558

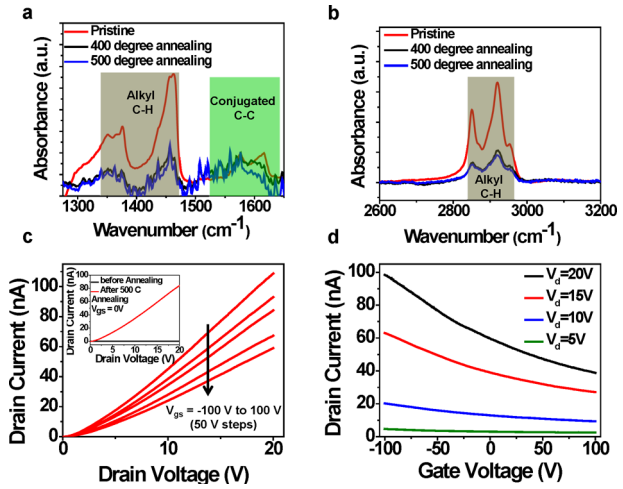

Figure 3. (a,b) ATR-FTIR normalized spectra of pristine, 400 and 500 °C annealed GNR films showing relative intensity decrease in peaks associated with alkyl C−H bonds for annealed samples. (c) Current vs drain voltage (I−V_d) of a typical GNR film device under different gate voltages (V_{gs}). (d) Current vs gate voltage (I−V_{gs}) of the same device under different drain voltages (V_d). Inset shows the I−V_d of the device before and after annealing at 500 °C.

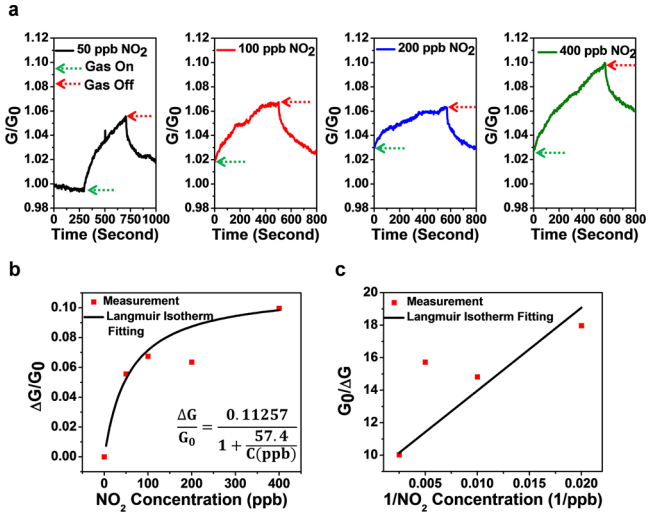

Figure 4. NO_2 gas sensing experiment using a GNR film device. (a) Time domain normalized conductance (G/G_0) of the GNR film device during introduction of different concentrations of NO_2. Green arrows correspond to the device being exposed to a certain concentration of NO_2, while red arrows correspond to the device being flushed with Ar only. (b) Measured conductance change ($\Delta G/G_0$) of the device in (a) as a function of NO_2 concentration (red squares) and the corresponding Langmuir isotherm curve fitting (black line). Langmuir isotherm fitted equation is written in the bottom right corner. (c) Inverse conductance change ($G_0/\Delta G$) vs inverse NO_2 concentration, showing a linear relation that further confirms Langmuir isotherm fitting.

was carried out to examine the effect of annealing on GNR quality, which revealed no apparent extra defects induced by the thermal treatment (Figure s3). Figure 3c,d shows the current vs drain voltage (I−V_d) and current vs gate voltage (I−V_{gs}) of a GNR film device after annealing at 500 °C. Figure 3c inset shows I−V_d for a thin-film device before (black curve) and after (red curve) annealing at 500 °C, which confirms that annealing can increase the conduction significantly. Although the GNR is semiconducting, the limited p-type current modulation may be attributed to an electric field screening effect in thick (i.e., 30−100 nm) GNR films and relatively high ribbon-to-ribbon junction resistance (Note s2).[30,31]

To demonstrate the applicability of GNR film devices, we used a GNR film device as a NO_2 gas sensor. High sensitivity to NO_2 is very crucial for human health, as relatively low concentrations (i.e., 0.2 ppm) can cause respiratory irritation.[32] For sensor measurements, we used Ar as a dilution gas for different NO_2 concentrations and exposed the device to different concentrations while monitoring the relative conductance (G/G_0) as a function of time (G is the absolute conductance of the device at any given time and G_0 is the initial conductance of the device before sensing). After the device is exposed to a certain NO_2 concentration (green arrow), G/G_0 increases by electron extraction from NO_2 molecules (Figure 4a). Then, the sensing chamber is flushed with Ar to remove NO_2 from the chamber (red arrow) and recover G/G_0 before the new concentration is introduced in the chamber. The conductance change of a device is defined as $\Delta G/G_0 = (G - G_0)/G_0$ and is considered a metric for device sensitivity for a certain concentration. The dependence of $\Delta G/G_0$ on the NO_2 concentration is plotted in Figure 4b,c. The fitted Langmuir isotherm indicates charge transfer as the sensing mechanism for GNR film devices. We note that the data point for 200 ppb NO_2 exposure is an outlier compared to the rest of the data, and the reason may be related to uncontrolled temporal perturbation to the device. Our GNR film sensors exhibit high sensitivities, comparing favorably to other graphene-based NO_2 sensors.[33−35] For example, Novoselov et al.[33] and Kim et al.[35] reported $\Delta G/G_0 \approx 4\%$ and 0.7% for pristine graphene and ozone-treated graphene devices, respectively, exposed to NO_2 concentration of 1 ppm. On the other hand, we observed $\Delta G/G_0 \approx 5.6\%$ for NO_2 concentration of 50 ppb (Note s3).

In summary, a method was developed to deposit individual GNRs on SiO_2 using CHP as a solvent and dodecyltriethoxysilane for surface functionalization. AFM of individual deposited GNRs revealed GNRs with a length of >500 nm and a thickness of ∼0.78 nm. Additionally, Raman spectroscopy of individual deposited GNRs showed characteristic D, G, 2D, and D+D′ peaks, and electrical measurements on an individual GNR confirmed the conductivity of such GNRs. Moreover, GNR film devices were fabricated, and ATR-FTIR confirmed the partial removal of alkyl chains from the GNR edges upon annealing the devices at 400 and 500 °C, which was further supported by the significant conductance increase of GNR film devices. Furthermore, we have demonstrated the exceptional NO_2 sensing performance of the GNR film device. The GNR film-based sensor is sensitive to low NO_2 concentrations down to 50 ppb.

■ ASSOCIATED CONTENT

Supporting Information

UV−vis absorption of GNR dispersions (Figure s1), AFM images of GNRs (Figure s2), Raman spectrum of GNR films under different annealing temperatures (Figure s3), more ATR-FTIR spectra (Figure s4), experimental methods (Note s1), discussion about GNR device study (Note s2), and discussion about GNR film sensing (Note s3). This material is available free of charge via the Internet at http://pubs.acs.org.

dx.doi.org/10.1021/ja502764d | J. Am. Chem. Soc. 2014, 136, 7555−7558

AUTHOR INFORMATION

Corresponding Author

chongwuz@usc.edu

Author Contributions

[§]A.N.A. and G.L. contributed equally.

Notes

The authors declare no competing financial interest.

ACKNOWLEDGMENTS

We acknowledge the Office of Naval Research, European Research Council grant on NANOGRAPH, DFG Priority Program SPP 1459, and European Union Projects UPGRADE, GENIUS, and MoQuaS for financial support.

REFERENCES

(1) Son, Y.-W.; Cohen, M. L.; Louie, S. G. *Phys. Rev. Lett.* **2006**, *97*, 216803.
(2) Han, M. Y.; Özyilmaz, B.; Zhang, Y.; Kim, P. *Phys. Rev. Lett.* **2007**, *98*, 206805.
(3) Liang, X.; Wi, S. *ACS Nano* **2012**, *6*, 9700−9710.
(4) Abbas, A. N.; Liu, G.; Liu, B.; Zhang, L.; Liu, H.; Ohlberg, D.; Wu, W.; Zhou, C. *ACS Nano* **2014**, *8*, 1538−1546.
(5) Son, J. G.; Son, M.; Moon, K.-J.; Lee, B. H.; Myoung, J.-M.; Strano, M. S.; Ham, M.-H.; Ross, C. A. *Adv. Mater.* **2013**, *25*, 4723−4728.
(6) Wang, X.; Dai, H. *Nat. Chem.* **2010**, *2*, 661−665.
(7) Wang, X.; Ouyang, Y.; Li, X.; Wang, H.; Guo, J.; Dai, H. *Phys. Rev. Lett.* **2008**, *100*, 206803.
(8) Li, X.; Wang, X.; Zhang, L.; Lee, S.; Dai, H. *Science* **2008**, *319*, 1229−1232.
(9) Bai, J.; Duan, X.; Huang, Y. *Nano Lett.* **2009**, *9*, 2083−2087.
(10) Abramova, V.; Slesarev, A. S.; Tour, J. M. *ACS Nano* **2013**, *7*, 6894−6898.
(11) Kato, T.; Hatakeyama, R. *Nat. Nanotechnol.* **2012**, *7*, 651−656.
(12) Sokolov, A. N.; Yap, F. L.; Liu, N.; Kim, K.; Ci, L.; Johnson, O. B.; Wang, H.; Vosgueritchian, M.; Koh, A. L.; Chen, J.; Park, J.; Bao, Z. *Nat. Commun.* **2013**, *4*, 2402.
(13) Pan, Z.; Liu, N.; Fu, L.; Liu, Z. *J. Am. Chem. Soc.* **2011**, *133*, 17578−17581.
(14) Solís-Fernández, P.; Yoshida, K.; Ogawa, Y.; Tsuji, M.; Ago, H. *Adv. Mater.* **2013**, *25*, 6562−6568.
(15) Wei, D.; Xie, L.; Lee, K. K.; Hu, Z.; Tan, S.; Chen, W.; Sow, C. H.; Chen, K.; Liu, Y.; Wee, A. T. S. *Nat. Commun.* **2013**, *4*, 1374.
(16) Xie, L.; Wang, H.; Jin, C.; Wang, X.; Jiao, L.; Suenaga, K.; Dai, H. *J. Am. Chem. Soc.* **2011**, *133*, 10394−10397.
(17) Jiao, L.; Zhang, L.; Wang, X.; Diankov, G.; Dai, H. *Nature* **2009**, *458*, 877−880.
(18) Pan, M.; Girao, E. C.; Jia, X.; Bhaviripudi, S.; Li, Q.; Kong, J.; Meunier, V.; Dresselhaus, M. S. *Nano Lett.* **2012**, *12*, 1928−1933.
(19) Cai, J.; Ruffieux, P.; Jaafar, R.; Bieri, M.; Braun, T.; Blankenburg, S.; Muoth, M.; Seitsonen, A. P.; Saleh, M.; Feng, X.; Müllen, K.; Fasel, R. *Nature* **2010**, *466*, 470−473.
(20) Ruffieux, P.; Cai, J.; Plumb, N. C.; Patthey, L.; Prezzi, D.; Ferretti, A.; Molinari, E.; Feng, X.; Müllen, K.; Pignedoli, C. A.; Fasel, R. *ACS Nano* **2012**, *6*, 6930−6935.
(21) Schwab, M. G.; Narita, A.; Hernandez, Y.; Balandina, T.; Mali, K. S.; De Feyter, S.; Feng, X.; Müllen, K. *J. Am. Chem. Soc.* **2012**, *134*, 18169−18172.
(22) Koch, M.; Ample, F.; Joachim, C.; Grill, L. *Nat. Nanotechnol.* **2012**, *7*, 713−717.
(23) Tan, Y.-Z.; Yang, B.; Parvez, K.; Narita, A.; Osella, S.; Beljonne, D.; Feng, X.; Müllen, K. *Nat. Commun.* **2013**, *4*, 2646.
(24) Jensen, S. R. A.; Ulbricht, R.; Narita, A.; Feng, X.; Müllen, K.; Hertel, T.; Turchinovich, D.; Bonn, M. *Nano Lett.* **2013**, *13*, 5925−5930.
(25) Kim, K. T.; Jung, J. W.; Jo, W. H. *Carbon* **2013**, *63*, 202−209.
(26) Kim, K. T.; Lee, J. W.; Jo, W. H. *Macromol. Chem. Phys.* **2013**, *214*, 2768−2773.
(27) Vo, T. H.; Shekhirev, M.; Kunkel, D. A.; Morton, M. D.; Berglund, E.; Kong, L.; Wilson, P. M.; Dowben, P. A.; Enders, A.; Sinitskii, A. *Nat. Commun.* **2014**, *5*, 3189.
(28) Narita, A.; Feng, X.; Hernandez, Y.; Jensen, S. R. A.; Bonn, M.; Yang, H.; Verzhbitskiy, I. A.; Casiraghi, C.; Hansen, M. R.; Koch, A. H. R.; Fytas, G.; Ivasenko, O.; Li, B.; Mali, K. S.; Balandina, T.; Mahesh, S.; De Feyter, S.; Müllen, K. *Nat. Chem.* **2014**, *6*, 126−132.
(29) Osella, S.; Narita, A.; Schwab, M. G.; Hernandez, Y.; Feng, X.; Müllen, K.; Beljonne, D. *ACS Nano* **2012**, *6*, 5539−5548.
(30) Do, J.-W.; Estrada, D.; Xie, X.; Chang, N. N.; Mallek, J.; Girolami, G. S.; Rogers, J. A.; Pop, E.; Lyding, J. W. *Nano Lett.* **2013**, *13*, 5844−5850.
(31) Sangwan, V. K.; Ortiz, R. P.; Alaboson, J. M. P.; Emery, J. D.; Bedzyk, M. J.; Lauhon, L. J.; Marks, T. J.; Hersam, M. C. *ACS Nano* **2012**, *6*, 7480−7488.
(32) Threshold limit values (TLVs) and biological exposure indices (BEIs): ACGIH. Nitrogen Dioxide. *2012 TLVs and BEIs*; ACGIH: Cincinnati, OH, 2012.
(33) Schedin, F.; Geim, A. K.; Morozov, S. V.; Hill, E. W.; Blake, P.; Katsnelson, M. I.; Novoselov, K. S. *Nat. Mater.* **2007**, *6*, 652−655.
(34) Pearce, R.; Iakimov, T.; Andersson, M.; Hultman, L.; Spetz, A. L.; Yakimova, R. *Sens. Actuators, B* **2011**, *155*, 451−455.
(35) Chung, M. G.; Kim, D. H.; Lee, H. M.; Kim, T.; Choi, J. H.; Seo, D. K.; Yoo, J.-B.; Hong, S.-H.; Kang, T. J.; Kim, Y. H. *Sens. Actuators, B* **2012**, *166−167*, 172−176.